Crystal structure analysis and first principle investigation of F doping in $LiFePO_4$

Miloš Milović [a], Dragana Jugović [a*], Nikola Cvjetićanin [b], Dragan Uskoković [a], Aleksandar S. Milošević [c], Zoran S. Popović [c], Filip R. Vukajlović [d]

[a] Institute of Technical Sciences of SASA, Knez Mihailova 35/IV, 11 000 Belgrade, Serbia

[b] Faculty of Physical Chemistry, University of Belgrade, Studentski trg 12-16, P.O. Box 137, Belgrade, Serbia

[c] Vinča Institute of Nuclear Sciences (020), University of Belgrade, P.O. Box 522, RS-11001 Belgrade, Serbia

[d] Vinča Institute of Nuclear Sciences (020), P.O. Box 522, RS-11001 Belgrade, Serbia

Abstract

This work presents the synthesis of F-doped $LiFePO_4$/C composite by the specific modification of the recently suggested synthesis procedure based on an aqueous precipitation of precursor material in molten stearic acid, followed by a high temperature treatment. Besides the lattice parameters and the primitive cell volume reductions, compared to the undoped sample synthesized under the same conditions, the Rietveld refinement also shows that fluorine ions preferably occupy specific oxygen sites. Particularly, the best refinement is accomplished when fluorine ions occupy O(2) sites exclusively. By means of up-to-date electronic structure and total

energy calculations this experimental finding is theoretically confirmed. Such fluorine doping also produces closing of the gap in the electronic structure and consequently better conductivity properties of the doped compound. In addition, the morphological and electrochemical performances of the synthesized powder are fully characterized.

Keywords: Lithium iron phosphate ($LiFePO_4$), Rietveld analysis, Fluorine doping, Cathode, Electronic band structure

*Corresponding author: Dragana Jugović

Institute of Technical Sciences of SASA

Knez Mihailova 35/IV, 11 000 Belgrade, Serbia,

Phone: +381641177549,

Fax: +381112185263,

e-mail: dragana.jugovic@itn.sanu.ac.rs; djugovic@vinca.rs

1. Introduction

In the on-going search for alternative cathode materials for Li-ion batteries, olivine-type lithium iron orthophosphate ($LiFePO_4$) is one of the most promising candidates due to its high energy density (with the theoretical capacity of 170 $mAhg^{-1}$ and plateau voltage of 3.5 V vs. Li^+/Li), high safety, both electrochemical and thermal stability, environmental appropriateness and low raw materials cost. However, despite its numerous advantages this material suffers from poor rate performance due to its inherent conducting properties – low electronic conductivity coupled with slow diffusion rate of lithium ions [1]. This issue has become a huge obstacle for

extensive applications of olivine-phosphate in high power rate devices such as hybrid electric vehicles and electric vehicles. Up until now, many efforts have been made to overcome such an obstacle. Generally, there are three different approaches to enhance electrochemical performance of $LiFePO_4$: (i) introduction of conductive additives, e.g., carbon coating of active material particles in $LiFePO_4$/C composite; (ii) particle size minimization and morphology control; and (iii) ion doping [2-6].

Various ions have been used as dopants in $LiFePO_4$ [7-15]. Depending on the type of the doping material one can have an anion or a cation doping. Cation doping at Li, or Fe sites, has been widely investigated and debated [7-9, 12]. On the other hand, the anion doping of $LiFePO_4$ has been rarely investigated and has started only recently [10, 11, 13-15]. Earlier papers devoted to the layered structure cathode materials [16, 17] inspired these works. The rate capability has been improved by the fluorine substitutions at oxygen sites, as well as capacity retention and cycle stability of $Li(M_{1x}M_{2y}M_{3z})O_2$ ($M_{1,2,3}$ = Co, Ni, Mn and x+y+z=1) layered materials. It appears that anion doping has also improved the electrochemical performance of $LiFePO_4$. Namely, the doping of $LiFePO_4$ with F^-, Cl^- and S^{2-} gave very satisfactory results (cf., for instance, [13-15]).

Liao et al. [11] were among the first who investigated the effects of fluorine substitution on electrochemical behavior of $LiFePO_4$/C cathode. They concluded that F-substitution improved both the high rate capability and the cycling life at high temperatures, as compared with the pure material. Enhanced high rate performance and improved cycle stability of F-doped olivine-phosphate was also reported in the very recent studies [13, 18, 19]. However, there exists the uncertainty about the site in the crystal lattice, which the fluorine ion occupy. Two proposals were given: (i) the first one suggested that $3F^-$ ions replace PO_4^{3-} group as a whole [11, 13], and (ii) the second one declared that F^- could only be replaced at the oxygen sites [18, 19].

Considering the second proposition, there are three nonequivalent randomly occupied O sites (namely O(1), O(2) and O(3) site) in the crystalline elementary cell of $LiFePO_4$ [20]. The first principles computational results indicate that electronic properties, the lithium insertion voltage and general electrochemical behavior are very sensitive to the placement of fluorine ions in the structure of this compound [10]. Owing to that, it is very important to determine the most probable positions of the fluorine replacements in the lattice of $LiFePO_4$.

To the best of the author's knowledge there do not exist careful investigations of the most probable fluorine replacement sites in olivine compounds, as well as the exact stoichiometry of such fluorine doping. Earlier theoretical investigation of $Li_{0.5}FePO_{3.5}F_{0.5}$ (12.5 % of oxygen is replaced by fluorine) [10], took improbably high content of fluorine, which is very non-trivial to obtain experimentally.

The structure of $LiFePO_4$ (Fig. 1.) belongs to the orthorhombic space group *Pnma* (#62), consisting of a slightly distorted hexagonal close-packed (hcp) oxygen framework. The phosphorous atoms occupy 1/8 of tetrahedral sites, while lithium and iron atoms occupy 1/2 of octahedral sites (denoted as M(1) and M(2) sites, respectively). The edge-shared LiO_6 octahedra form linear chains running parallel to the b-axis; the FeO_6 form zigzag planes of corner-shared octahedra in the b-c planes. The PO_4 tetrahedra bridge between adjacent M(2) planes in the olivine structure.

In the present paper, F-doped $LiFePO_4$/C composite was synthesized by means of the newly suggested simple method, which was based on an aqueous co-precipitation of an Fe(II) precursor material in molten stearic acid followed by high temperature treatment. The effects of F-doping on the crystal structure were investigated in details and compared with the previously published results for the undoped $LiFePO_4$/C powder prepared under the same synthesis conditions [21]. In addition, morphological and electrochemical properties of the synthesized

powder were investigated. Special attention has been paid to the refinement of the crystal structure of the synthesized powdered samples. The careful refinement of the X-ray diffraction data has indicated that fluorine ions prefer specific oxygen site in the crystal structure. In order to check our experimental findings concerning the most probable placement of fluorine into lithium iron orthophosphate, we investigated theoretically the electronic structure and crystal stability of both pure $LiFePO_4$ and fluorine doped compound, which we modeled by orthorhombic $LiFePO_{3.75}F_{0.25}$ compound. This has been done on the basis of density functional theory (DFT) with the generalized gradient approximation (GGA).

The rest of the paper is organized as follows. After summarizing the basics of the olivine type lithium iron orthophosphate as an alternative for cathode material of Li-ion type batteries and the earlier attempts to dope this material, the essential experimental conditions for the synthesis of $LiFePO_{3.98}F_{0.02}$/C and the experimental methods used for the characterization of the physical, chemical and electrochemical properties of this compound are given in Sec. 2, together with the thorough discussion of these results. The computational details used in our first principles simulations, jointly with the theoretical results relevant for comparisons with experiments, can be found in Sec. 3. Section 4 gives brief conclusion.

2. Experimental

2.1 Experimental Details

F-doped $LiFePO_4$/C composite powder was synthesized by aqueous precipitation in the presence of stearic acid and subsequent heat treatment. Synthesis procedure was the same as previously implemented for the synthesis of the undoped $LiFePO_4$/C composites [21], except for lithium source. The starting materials were $(NH_4)_2HPO_4$, $FeSO_4 \cdot 7H_2O$, LiF, and stearic acid, mixed in equimolar quantities. This time LiF has served as both lithium and fluorine source. The

obtained precursor powder was calcined at the temperature of 700 °C for 3 hours in a flowing, slightly reductive atmosphere (Ar + 5%H_2), then washed in distilled water and dried under vacuum.

X-ray diffraction data were collected on the Philips PW 1050 diffractometer with Cu-K$\alpha_{1,2}$ radiation (Ni filter) at the room temperature. Measurements were done in 2θ range of 15-110° with step size of 0.02° and counting time of 14 s per step. Crystal structure refinement was based on the Rietveld full profile method [22] using Koalariet software [23].

The morphology of the synthesized powder was analyzed by field emission scanning electron microscopy (FESEM, Supra 35 VP, Carl Zeiss). More detailed analysis of particle microstructure was accomplished using transmission electron microscopy (JEOL JEM 2000 FX) with acceleration voltage of 200 keV.

The particle size analyzer (PSA) Mastersizer 2000 (Malvern Instruments Ltd., UK) has been used for the determination of the particle size distributions.

Chemical composition of the final powder was determined by the ICP-AES measurements combined with SA720 ion selective electrode (ISE) analysis. The ICP-AES measurements were performed by simultaneous ICP-AES using a Thermo Scientific iCAP-6500 DUO ICP (Thermo Fisher Scientific, UK) spectrometer.

Electrochemical measurements were carried out in a closed, argon filled two-electrode cell, with metallic lithium as a counter electrode. 1M solution of $LiClO_4$ (p.a., Chemmetall GmbH) in PC (p.a., Honeywell) was used as electrolyte. Working electrodes were made from synthesized material, carbon black and polyvinylidene fluoride (PVdF, Aldrich) mixed in 75:15:10 weight percent ratio and deposited on platinum foils from slurry prepared in N-methyl-2-pyrrolidone. Galvanostatic charge/discharge tests were performed between 2.3 and 4.1 V at different current rates by using Arbin BT 2042 battery test system.

2.2 Experimental Results and Discussion

The morphology of the powder, revealed by scanning electron microscopy, is shown in Fig. 2. The particles are irregular in shape, highly agglomerated with nodular structures, quite similar to the morphology of the undoped powder [21]. Particle bonding and neck formation, denoting inter-particle sintering, can be observed as well. Apparently, the morphology of the powder was not affected by fluorine doping. The particle size distribution (PSD) curve of the powder (Fig. 3) has a lognormal shape with a high degree of uniformity, showing span value of 1.2 and mean particle size of 330 nm.

X-ray powder diffraction pattern (Fig. 4) was used for both phase identification and structural analysis. Olivine structured $LiFePO_4$ is obtained as a major phase, with small amount (roughly 2 wt.%) of gamma-Li_3PO_4 and $Fe_2P_2O_7$ phases. These unwanted products are almost certainly caused by slightly exceeded gas reductivity as a consequence of the thermal treatment. During pyrolytic degradation, stearic acid decomposes to carbon, creating at the same time more reductive atmosphere that prevents the iron oxidation and the formation of Fe^{3+} sites [24]. Chemical analysis of the powder gave Li:Fe:P:F molar ratio of 0.98:1:1:0.02, respectively. There is no evidence of a crystalline carbon, so internal carbon could be treated as a contribution to the background. The amount of an in situ formed carbon (5 wt.%) was determined by heating the powder in air considering that only Fe^{2+} ions oxidize and contribute to the weight gain [25].

Rietveld refinement was performed using Koalariet computing program based on a fundamental parameters convolution approach to generate line profiles [23]. The structure of fluorine doped $LiFePO_4$ powder has been refined in the space group *Pnma* (D_{2h}^{16}) in olivine type with the following crystallographic positions: Li^+ ions in the crystallographic position 4*a* [0,0,0] with the local symmetry ī; Fe^{2+} and P^{5+} ions occupy two nonequivalent 4*c* crystallographic

positions [*x*,0.25,*z*] with local symmetry *m*. Oxygen O^{2-} ions occupy three different crystallographic positions: additional two 4*c* positions and one general 8*d* position [*x*,*y*,*z*] with local symmetry 1.

The Rietveld refinement results (Tables 1) indicate lattice parameters and primitive cell volume reduction compared to the undoped sample synthesized under the same conditions [21]. This is the indication that F^- ions are incorporated in the lattice, since F^- ionic radius is smaller than O^{2-} one ($r^{VI}(F^-)$ = 1.33 Å, $r^{VI}(O^{2-})$ = 1.40 Å [26]). Furthermore, doping with fluorine resulted in increased crystallite size in comparison with the undoped compound. Comparing the mean particle size estimated from PSD (Fig. 3), with the mean crystallite size from Table 1, one can conclude that these particles are of polycrystalline type made up of many crystallites.

Concerning fluorine ion, it is natural to presume that it substitutes one of the oxygen ions, rather than the whole $(PO_4)^{3-}$ group, as it has been stated in [11, 13]. Additionally, positively charged V_{PO4}^{3+} defect has very high formation energy [27], and therefore it is quite unlikely to expect such a substitution. There are three nonequivalent O sites (usually denoted as O(1), O(2), and O(3)) in the olivine lattice that may be occupied by fluorine ions. During the refinement procedure fluorine ions were free to occupy any of the three allowed O sites. The best refinement was accomplished when fluorine ions occupied O(2) sites exclusively, while the total site occupancy of that position for oxygen and fluorine ions was constrained to unity. The refined value of dopant concentration matches well, within the experimental error, with the fluorine concentration obtained by chemical analysis (two mole percents: $LiFePO_{3.98}F_{0.02}$). At the beginning we had much more fluorine in the precursor. However, fluorine ions usually sublime in open systems, with a gas flowing during the formation of olivine phase, so its actual concentration in the synthesized compound is much smaller than the nominal concentration in the precursor powder.

The Rietveld refinement has also shown additional electron density on the lithium sites indicating the formation of the so-called "antisite" defect. This is the defect in which the Li ion (on the M(1) site) and the Fe ion (on the M(2) site) are interchanged, thus creating Fe_{Li}^{+}-Li_{Fe}^{-} antisite pair. This antisite disorder (ca. 1-2 mol %) is believed to be intrinsic property of olivine $LiFePO_4$ [28]. It seems that fluorine doping leads to a slight reduction in the concentration of Li-Fe antisite defects (cf. Table 1). However, from the Rietveld refinement of the X-ray diffraction data, we cannot discriminate between the formation of antisite defects and the usual lithium deficiency, due to the well-known small X-ray atomic scattering factor of lithium ions.

Both refined and fixed fractional atomic coordinates (Table 2) were used for the calculation of all relevant bond distances and bond angles that enabled us to determine the coordination polyhedra. Relevant bond distances for undoped and doped powders are provided in Table 3. The calculated P-O(2) distance is significantly shorter, implying the presence of fluorine ion at the specific O(2) site, while the Fe–O(2) distance is consequently longer due to the Fe-O-P inductive effect. The PO_4 tetrahedron is distorted because of the presence of one short and one stretched P–O bond equal to 1.5044 Å and 1.6130 Å, respectively. The average P–O distance of 1.569 Å is consistent with the value of 1.55 Å estimated from the effective ionic radii of the four-coordinated P^{5+} and O^{2-} [26]. In the introductory part we mentioned that PO_4 tetrahedra bridge between adjacent M(2) planes in the olivine structure. More specifically, three of four oxygen ions of PO_4 tetrahedron (namely O(1), and two O(3)) lie in the same zigzag M(2) layer, while the fourth oxygen (that is O(2)) belongs to the adjacent M(2) layer (cf. Fig. 1). As a consequence, these PO_4 tetrahedrons practically define the free volume for the Li-ions movement. It is interesting to observe that the closest atomic site to the lithium ‘channel’ is the O(2) oxygen site.

In order to perform detailed analysis of the microstructure of the synthesized powder we used images obtained on the basis of transmission electron microscopy (TEM), which are given

in Figs. 5 and 6. The significant particle agglomeration is evident from the image depicted in Fig. 5. Therein, the grain boundaries are not quite clear and because of that the size of the individual primary particles is hard to estimate from this figure. Magnifying the specific part of the thin particle edge of our sample, by means of high resolution TEM (HRTEM), we were able to reveal the amorphous carbon film there. This carbon film is 3 nm thick and it is deposited on the (121) crystal plane of orthorhombic $LiFePO_4$ (Fig. 6). Accordingly, we can conclude that carbon nicely coats the synthesized olivine particles during the pyrolytic degradation of stearic acid producing, as a consequence, well-known improvement of the electrical conductivity of the synthesized powders.

The electrochemical performance of our sample, used as a cathode in a two-electrode cell, was examined by the charge-discharge tests. The galvanostatic cyclings were done with the same current rate, for both charging and discharging processes. The voltage vs. capacity discharge curves for different discharge rates are depicted in Fig. 7. The discharge rates are given in C/n, where C is the nominal capacity equal to 170 $mAhg^{-1}$, and n is the discharge time given in hours needed for the complete discharge. Flat plateaus widths in the region around 3.4 V, observed during the discharge, are decreasing with increasing the current rate. Almost theoretical value of 164 $mAhg^{-1}$ has been reached when 0.1C current was used for the discharging. It is also evident from Fig. 7 that reversible capacity at variable discharge rates shows excellent rate capability, during the cycling process.

3. Theoretical method

3.1 Computational Details

The spin unrestricted density functional theory (DFT) calculations for antiferromagnetic (AF) ordering were carried out firstly for the experimental lattice parameters of $LiFePO_4$ [21] using the full potential linearized augmented plane wave (FP-LAPW) method as implemented in the WIEN2K code (Blaha et al. Ref. 29). The unit cell is partitioned into non-overlapping muffin-tin spheres around the atomic sites and interstitial region. For these two regions different basis sets were used and the Kohn-Sham equations were solved self-consistently on an 2x4x6 **k**-mesh in the first Brillouin zone (BZ) resulting in 48 **k**-points. The exchange correlation potential was treated using: (a) the generalized gradient approximation (GGA) as parametrized by Perdew et al. [30] (we will refer to this calculation as PBE) and (b) the Tran-Blaha recipe [31] applied on a modified version of the Becke and Johnson exchange potential [32] for a more appropriate calculation of the band gap (we will refer to this calculation as TB-mBJ). The muffin-tin radii (R_{MT}) were 1.84 bohrs for Li, 1.89 bohrs for Fe, and 1.32 bohrs for P and O. Same radii were also used for determining the weighting of the partial densities of states for each atomic type and for integrating the net electron spin within each muffin-tin sphere. The parameter $R_{KMAX} = R_{MT} * K_{MAX}$ determines convergence, where R_{MT} is the smallest muffin-tin sphere radius and K_{MAX} is the plane wave cut-off. We take this parameter to be $R_{KMAX} = 7$ while the reciprocal space truncation was controlled by parameter G_{MAX} for which we used 12 $Bohr^{-1}$. For the self-consistency cycle we used two convergence criteria: $\Delta E_{tot} < 10^{-4}$Ry and $\Delta q < 10^{-4}$e (where e is the elementary charge). All graphs obtained on the basis of the FP-LAPW were produced with the Gaussian broadening of 0.04 eV. The scissors operator, which shifts the conduction band bottom, was not applied.

The spin polarized AF calculations were also performed with the GPAW computer code [33], based on real space grid implementation of the projector augmented wave (PAW) method with the grid spacing of 0.15 Å [34, 35]. This method has been used for the extensive relaxation

investigations because it is much faster than FP-LAPW method. The electronic exchange and correlation effects were described again using the PBE functional [30]. The calculations reported in this work were performed both for the experimental crystal structure of olivine-type lithium iron orthophosphate [20, 21], as well as for the properly relaxed pure $LiFePO_4$ and doped $LiFePO_{3.75}F_{0.25}$ (with one oxygen ion, out of sixteen, replaced with fluorine at three different possible oxygen positions: O(1), O(2) or O(3)). Atomic positions of all atoms are relaxed until force components on atoms were smaller than 0.05 eV/Å. The structure optimization was carried out utilizing the BFGS (Broyden–Fletcher–Goldfarb–Shanno) algorithm [36]. The calculations for pure $LiFePO_4$ started by employing an orthorhombic unit cell with 28 atoms in four formula units (space group *Pnma* (#62)), whose experimental lattice parameters are given in Table 1. The sampling of the corresponding Brillouin zone was done with 8 (2x2x2) Monkhorst-Pack special **k**-points and the Fermi temperature broadening of 0.1 eV [37]. Additional convergence tests were also done with 32 (2x4x4) **k**-points and the Fermi temperature of 0.03 eV. In the current work we have chosen the AF ordering which preserves the inversion symmetry, present in the paramagnetic state. Bearing in mind that our main goal here is to investigate the most favourable place for fluorine to substitute oxygen in the olivine-type lithium iron orthophosphate, this will not be a serious limitation. Especially, if one takes into account earlier very small differences between the relaxed parameters and total energies obtained for various possible AF orderings in pure $LiFePO_4$ [38].

In order to estimate the influence of pronounced electronic correlations, characteristic for this compound, we also did additional test calculations for both pure and doped olivine with the effective Hubbard U_{eff}= 4.3 eV correlation correction included at Fe sites in the framework of so-called DFT + *U* approach, as implemented by Anisimov et al. [39, 40]. We will refer to these

calculations as PBE+*U* calculations (many workers refer to such calculations also as GGA+*U* calculations).

3.2 Theoretical Results and Discussion

The antiferromagnetic calculations, with the same spins on sites related by inversion symmetry within crystalline unit cell, were performed on the basis of two different methods: FP-LAPW and PAW.

Firstly, we did FP-LAPW calculations (PBE, PBE+*U* and TB-mBJ) with *experimental* values for lattice parameters and atomic positions (cf. Table 1, and Refs. 20 and 21). The one-electron spectra in terms of total and partial densities of states (DOS) can give us a qualitative picture of various contributions to the self-consistent results and of the bonding characteristics of the pure and fluorine doped olivine compounds. Figures 8 and 9 show total and the atom-resolved partial density of states for pure $LiFePO_4$ and doped $LiFePO_{3.75}F_{0.25}$ with one oxygen atom (out of sixteen) at the O(2) position changed with fluorine. While phosphorous and lithium atoms are just giving their valence electrons without much hybridization with other atoms, oxygen *p* and iron *d* states hybridization produces certain order of covalence of Fe-O bonds. The dominant electronic character near the Fermi level is due to Fe 3*d* states, and a noticeable mixing with O 2*p* states is apparent approximately between –4 eV and –2 eV. Minority Fe 3*d* states are located in the narrow region around the band gap with practically no mixing with O or other cations in pure $LiFePO_4$. The same is true for one fluorine atom substitution of oxygen O(2) atom, except for the Fermi level shift in the region of finite density of minority Fe *d* states with the consequent improvement in the electronic conductivity of doped $LiFePO_{3.75}F_{0.25}$. While the pure compound is an insulator with a tiny band gap within PBE, and more appropriate gap values with additional

exchange-correlation corrections included in the framework of PBE+*U* and TB-mBJ, the fluorine-doped olivine has finite density of states (DOS) at the Fermi level for both PBE and PBE+*U* exchange-correlation functionals used. As a consequence, in the doped compound the band gap disappears, although the DOS is not too high in that region. Table 4 lists the gap values and the magnetic moments at all atomic sites obtained by means of the three upper mentioned exchange-correlation functionals for pure $LiFePO_4$. Table 5 lists the magnetic moments at atomic sites obtained by the use of PBE and PBE+*U* exchange-correlation functionals in $LiFePO_{3.75}F_{0.25}$. Let us note here that the half-metallic solution has been obtained for PBE exchange-correlation functional (cf. Fig. 9 which shows a gap in the down spin channel only). In order to show how the doping influence the character of electronic states around the gap, we have given the band structure results for antiferromagnetic $LiFePO_4$ and the doped $LiFePO_{3.75}F_{0.25}$ obtained by FP-LAPW with PBE, as well as the total density of states for $LiFePO_{3.75}F_{0.25}$, in the region [–2, 2] eV around the Fermi level (Fig. 10). Half-metallic solution is evident for the doped compound.

Secondly, we performed full structural optimization for the pure $LiFePO_4$ compound, by means of GPAW. That is, for pure compound we have relaxed both lattice parameters and atomic positions. The relaxation changes of lattice parameters for the doped $LiFePO_{3.75}F_{0.25}$, when one of the oxygen atoms in the unit cell is replaced by fluorine, have been insignificant. Therefore, the appropriately relaxed lattice parameters of the pure $LiFePO_4$ were used for olivine doped with fluorine and later on we only performed relaxation of the atomic positions. The relaxed volume of the crystal unit cell is 2% larger than the experimental unit cell volume (the relaxed lattice parameters are: a=10.404 Å, b= 6.049 Å and c= 4.726 Å).

The total energy of $LiFePO_4$ after fluorine doping at the O(2) site is 140 meV and 129 meV lower than if that substitution is made at the O(1) site O(3) site, respectively. This result is in accordance with our best Rietveld refinement achievement when fluorine ion was substituted

at the O(2) site. The Fe-F bond length is longer than the previous Fe-O bond. The quite significant distortion of the original FeO_6 octahedron is shown in Fig. 11. The crystal structure of olivine has three different types of oxygen atoms, which form octahedrons around Fe and Li atoms and tetrahedrons around P atoms. This compound has zigzag planes of corner-shared FeO_6 octahedra in the b-c planes. The PO_4 tetrahedron share common O(3)-O(3) edge with FeO_6 octahedron and common corner at O(1) position with another FeO_6 octahedron from the same Fe layer, therefore stabilizing the crystal structure in that iron layer. The O(2) atom is common corner of PO_4 tetrahedron and FeO_6 octahedron from adjacent zigzag Fe layer. These O(2) atoms are making connections between the different Fe layers and thus taking their part in backing up the crystal structure (Fig. 1). There are no direct superexchange paths between the Fe atoms in these planes and long-range interactions, such as Fe-O-P-O-Fe triple exchange, were suggested [20]. Longer exchange paths along this direction are probable reason for the small 52 K value of the Neel's AF transition temperature [20]. The O(2) atoms are the type of oxygen closest to the Li atomic channel. As such, they are probably prone to being replaced by fluorine at their positions because the extra free electrons, which appear in the system after doping, have come from lithium atoms and they are naturally striving to take the place of the closest oxygen. We are aware that this is just one extremely qualitative explanation of the reason why F substitution takes place at the O(2) sites.

Fig. 12 shows total AF density of states calculated for the relaxed atomic positions of doped $LiFePO_{3.75}F_{0.25}$ by using the GPAW method. Instead of insulating state characteristic for pure $LiFePO_4$ compound, we are getting a metallic solution with finite density of states at the Fermi energy. This metallic type solution endures even if we include Hubbard type U_{eff}= 4.3 eV correlation correction at the Fe sites. The extra electron, which appeared in the system after the substitution of one oxygen atom in the unit cell with fluorine, is striving to the iron atoms with

their unfilled *d* electronic states. We also present the partial density of states of Fe, O(2) and F in pure and doped olivine (Fig. 13). Note a quite insignificant overlapping between the fluorine and iron states. The change of the character of the states at the Fermi energy and increased mobility of electrons for fluorine-doped olivine will clearly enhance the chemical diffusion of Li ions in the doped compound.

One possibility to illustrate graphically the extra electron distribution through the elementary cell of the doped compound is to present the isosurface plots of the total charge density difference between fluorine-doped olivine $LiFePO_{3.75}F_{0.25}$ and pure $LiFePO_4$ ($\Delta\rho=\rho_{doped} - \rho_{pure}$). Fig. 14 depicts this density difference calculated using GPAW with PBE exchange-correlation functional. Note that the electron density of $LiFePO_4$ was calculated for the oxygen O(2) placed at the relaxed position of fluorine in doped $LiFePO_{3.75}F_{0.25}$. It is clearly seen from this figure that extra electron is leaving the atomic sphere around the fluorine atom (yellow contour) and is transferred mostly to the iron atoms (gray contours).

In order to represent our results in more quantitative terms, we offer in Table 6 the exact extra electron distribution between the atoms in the unit cell. Note that this extra electron is obtained by integration of total charge density between -0.4 eV and E_f, at the bottom of the conduction band.

4. Conclusions

F-doped lithium iron phosphate powder was successfully synthesized by facile precipitation in molten stearic acid, followed by thermal treatment. Crystal structure refinement showed that doping with fluorine ions preserves olivine structure, and that fluorine ions are solely

positioned at O(2**)** oxygen site. The obtained powder showed excellent electrochemical performances with high rate capability.

Theoretical modelings confirmed and support these experimental findings. The fluorine substitution of O(2) oxygen is energetically most stable solution. The obtained metallic solution (no matter how poor that metallic state could be) with the expected increase in mobility of electrons for fluorine-doped olivine will, without a doubt, enhance the chemical diffusion of Li ions and positively influence electrochemical performance of the doped compound. Since a substitution of one oxygen with one fluorine atom in the crystal unit cell breaks the inversion symmetry of a doped compound, we also got noticeable ferrimagnetic moment per unit cell on the order of $\sim 0.25\mu_B$, where μ_B is the Bohr magneton. This effect could be measured by SQUID magnetometer on the carefully synthesized samples (samples without magnetic impurities).

Acknowledgements: The authors express their thanks to: Dr. Miodrag Mitrić and Dr. Željko Šljivančanin for help and very valuable suggestions, Dr. Biljana Dojčinović for performing chemical analysis of synthesized samples, Dr. Marija Vukomanović and Dr. Danilo Suvorov for performing electron microscopy experiments. The Ministry of Education, Science and Technological Development of the Republic of Serbia provided financial support for this study under grants nos. III 45004, III45014, and OI 171033.

References

[1] L.X. Yuan, Z.H. Wang, W.X. Zhang, X.L. Hu, J.T. Chen, Y.H. Huang, J.B. Goodenough, Energy Environ. Sci. 4 (2011) 269-284.

[2] B.L. Ellis, K.T. Lee, L.F. Nazar, Chem. Mater. 22 (2010) 691-714.

[3] K. Zaghib, A. Guerfi, P. Hovington, A. Vijh, M. Trudeau, A. Mauger, J. B. Goodenough, C. M. Julien, J. Power Sources 232 (2013) 357-369.

[4] J. Y. Xiang, J. P. Tu, L. Zhang, X. L. Wang, Y. Zhou, Y. Q. Qiao, Y. Lu, J. Power Sources 195 (2010) 8331-8335.

[5] W. L. Liu, J. P. Tu, Y. Q. Qiao, J. P. Zhou, S. J. Shi, X. L. Wang, C. D. Gu, J. Power Sources 196 (2011) 7728-7735.

[6] J. Orlenius, O. Lyckfeldt, K. A. Kasvayee, P. Johander, J. Power Sources 213 (2012) 119-127.

[7] S.Y. Chung, J.T. Bloking, Y.M. Chiang, Nat. Mater. 1 (2002) 123-128.

[8] C.S. Sun, Z. Zhou, Z.G. Xu, D.G. Wang, J.P. Wei, X.K. Bian, J. Yan, J. Power Sources 193 (2009) 841-845

[9] M. Wagemaker, B.L. Ellis, D. Lützenkirchen-Hecht, F.M. Mulder, L.F. Nazar, Chem. Mater. 20 (2008) 6313-6315.

[10] M.E. Arroyo y de Dompablo, U. Amador, J.M. Tarascon, J. Power Sources 174 (2007) 1251-1257.

[11] X.Z. Liao, Y.S. He, Z.F. Ma, X.M. Zhang, L. Wang, J. Power Sources 174 (2007) 720-725.

[12] L. Pang, M. Zhao, X. Zhao, Y. Chai, J. Power Sources 201 (2012) 253-258.

[13] M. Pan, X. Lin, Z. Zhou, J. Solid State Electrochem. 16 (2011) 1615-1621.

[14] C.S. Sun, Y. Zhang, X.J. Zhang, Z. Zhou, J. Power Sources 195 (2010) 3680-3683.

[15] S.B. Lee, S.H. Cho, V. Aravindan, H.S. Kim, Y.S. Lee, Bull. Korean Chem. Soc. 30 (2009) 2223-2226.

[16] H.S. Shin, S.H. Park, C.S. Yoon, Y.K. Sun, Electrochem. Solid-State Lett. 8 (2005) A559-A563.

[17] S.H. Kang, I. Belharouak, Y.K. Sun, K. Amine, J. Power Sources 146 (2005) 650-653.

[18] F. Lu, Y. Zhou, J. Liu, Y. Pan, Electrochim. Acta 56 (2011) 8833-8838.

[19] F. Pan, W. Wang, J. Solid State Electrochem. 16 (2011) 1423-1427.

[20] V.A. Streltsov, E.L. Belokoneva, V.G. Tsirelson, N.K. Hansen, Acta Cryst. B 49 (1993) 147-153.

[21] D. Jugović, M. Mitrić, M. Kuzmanović, N. Cvjetićanin, S. Škapin, B. Cekić, V. Ivanovski, D. Uskoković, J. Power Sources 196 (2011) 4613-4618.

[22] H.M. Rietveld, J. Appl. Cryst. 2 (1969) 65-71.

[23] R.W. Cheary, A. Coelho, J. Appl. Cryst. 25 (1992) 109-121.

[24] N. Ravet, M. Gauthier, K. Zaghib, J.B. Goodenough, A. Mauger, F. Gendron, C.M. Julien, Chem. Mater. 19 (2007) 2595-2602.

[25] S. Yang, Y. Song, P.Y. Zavalij, M.S. Whittingham, Electrochem. Commun. 4 (2002) 239-244.

[26] R.D. Shannon, C.T. Prewitt, Acta Cryst. B 25 (1969) 925-946.

[27] K. Hoang, M. Johannes, Chem. Mater. 23 (2011) 3003-3013.

[28] M.S. Islam, D.J. Driscoll, C.A.J. Fisher, P.R. Slater, Chem. Mater. 17 (2005) 5085-5092.

[29] P. Blaha, K. Schwarz, G.K.H. Madsen, D. Kvasnicka, J. Luitz, WIEN2k, An Augmented Plane Wave + Local Orbitals Program for Calculating Crystal Properties, Karlheinz Schwarz, Techn. Universitat Wien, Austria, 2001.

[30] J. P. Perdew, S. Burke, M. Ernzerhof, Phys. Rev. Lett. 77 (1996) 3865-3868.

[31] F. Tran, P. Blaha, Phys. Rev. Lett. 102 (2009) 226401(4).

[32] A.D. Becke, E.R. Johnson, J. Chem. Phys. 124 (2006) 221101(4).

[33] J. Enkovaara , C. Rostgaard, J.J. Mortensen, J. Chen, M. Dulak, L. Ferrighi et al., J. Phys. Condens. Matter. 22 (2010) 253202(24).

[34] P.E. Blochl, Phys. Rev. B. 50 (1994) 17953-17979.

[35] J.J. Mortensen, L.B. Hansen, K.W. Jacobsen, Phys. Rev. B. 71 (2005) 035109(11).

[36] D.C. Liu, J. Nocedal, Math. Program. B 45 (1989) 503-528.

[37] H.J. Monkhorst, J.D. Pack, Phys. Rev. B. 13 (1976) 5188-5192.

[38] S. Shi, C. Ouyang, Z. Xiong, L. Liu, Z. Wang, H. Li, D. Wang, L. Chen, X. Huang, Phys. Rev. B. 71 (2005**)** 144404(6).

[39] V.I. Anisimov, J. Zaanen, O.K. Andersen, Phys. Rev. B. 44 (1991) 943-954.

[40] A.I. Liechtenstein, V.I. Anisimov, J. Zaanen, Phys. Rev. B. 52 (1995) R5467-R5470.

Table 1. The final results of the Rietveld structural refinement.

	$LiFePO_4$ [21]	F-doped $LiFePO_4$
Lattice parameters (Å)	a = 10.3279(3) b = 6.0096(2) c = 4.6994(1)	a = 10.3288(5) b = 6.0065(3) c = 4.6934(3)
Primitive cell volume ($Å^3$)	V = 291.68(9)	V = 291.18(2)
Mean crystallite size (nm)	75(4)	85(9)
Li site occ. by Fe	0.019(5)	0.017(7)
O2 site occ. by F	-	0.03(1)
R factor (%)	Rwp = 3.76	Rwp = 1.74

Table 2. Fixed and refined atomic coordinates and isotropic displacement parameters.

Fractional coordinates	F-doped $LiFePO_4$			B ($Å^2$)
	x	y	z	
Li (4*a*)	0	0	0	2.7
Fe (4*c*)	0.2820(2)	0.25	0.9774(8)	1.4
P (4*c*)	0.0941(5)	0.25	0.4138(9)	0.4
O(1) (4c)	0.1059(10)	0.25	0.7423(11)	2.1
O(2) (4c)	0.4596(11)	0.25	0.2096(11)	2.1
O(3) (8d)	0.1690(9)	0.0380(10)	0.2822(10)	2.1

Table 3. Selected bond lengths (in Å).

M – O bond	$LiFePO_4$	F-doped $LiFePO_4$
Fe – O(1)	2.1593	2.1277
Fe – O(2)	2.1126	2.1341
Fe – O(3) x 2	2.2425	2.2424
Fe – O(3)' x 2	2.0425	2.0220
$(Fe – O)_{ave}$	2.1403	2.1318
Li – O(1) x 2	2.2288	2.2166
Li – O(2) x 2	2.0780	2.0704
Li – O(3) x 2	2.2018	2.2034
$(Li – O)_{ave}$	2.1695	2.1635
P – O(1)	1.5099	1.5466
P – O(2)	1.5218	1.5044
P – O(3) x 2	1.5954	1.6130
$(P – O)_{ave}$	1.5556	1.5692

Table 4. Calculated gap values and magnetic moments in Bohr magnetons (μ_B) at all atomic sites by use of FP-LAPW with *experimental* lattice parameters and PBE, PBE+*U* and mBJ exchange-correlation functionals for pure antiferromagnetic $LiFePO_4$.

	$\mu[\mu_B]$ PBE	$\mu[\mu_B]$ mBJ	$\mu[\mu_B]$ PBE+*U*
int.	0.00000	0.00000	0.00000
Li	-0.00059	-0.00022	-0.00046
Li	0.00059	0.00022	0.00046
Fe	3.38049	3.60538	3.53302
Fe	-3.38049	-3.60538	-3.53302
P	-0.00359	-0.00292	-0.00290
P	0.00359	0.00292	0.00290
O(1)	0.02814	0.02126	0.01982
O(1)	-0.02814	-0.02126	-0.01982
O(2)	0.02224	0.01745	0.01585
O(2)	-0.02224	-0.01745	-0.01585
O(3)	-0.02047	-0.001476	-0.01107
O(3)	0.02047	0.01476	0.01107
tot.	0.00000	0.00000	0.00000
Eg [eV]	0.508	2.782	2.845

Table 5. Calculated magnetic moments in Bohr magnetons (μ_B) at atomic sites by use of FP-LAPW with experimental lattice parameters and PBE, PBE+*U* and mBJ exchange-correlation functionals for doped olivine $LiFePO_{3.75}F_{0.25}$.

	μ [μ_B] PBE	μ [μ_B] PBE+*U*
int.	-0.01912	-0.05536
Li	-0.00054	-0.00057
Li	-0.00054	-0.00057
Li	0.00053	-0.00017
Li	0.00053	-0.00017
Fe1	3.10307	3.35806
Fe2	3.19215	3.45083
Fe3	-3.20630	-3.47467
Fe4	-3.28679	-3.51067
P	-0.00311	-0.00256
P	-0.00295	-0.00257
P	0.00004	-0.00120
P	0.00291	0.00257
O(1)	0.02809	0.01860
O(1)	0.02467	0.01915
O(1)	-0.01548	0.01995
O(1)	-0.02275	-0.01945
F	0.00899	0.00543
O(2)	0.01613	0.01430
O(2)	-0.02075	-0.01568
O(2)	-0.02121	-0.01609
O(3)	-0.02058	-0.01530
O(3)	-0.01678	-0.01297
O(3)	-0.01677	-0.01297
O(3)	-0.02058	-0.01530
O(3)	0.01082	0.00603
O(3)	0.01120	0.00727
O(3)	0.01120	0.00727
O(3)	0.01081	0.00602

cell -0.25309 -0.28068

Table. 6 The extra electron distribution between the atoms and the interstitial (Int.) region of the unit cell for doped olivine $LiFePO_{3.75}F_{0.25}$ obtained by an integration of the total charge density between -0.4 eV and E_f (cf. Fig. 9)[*)].

		Fe1	Fe2	Fe3	Fe4	F	Int.	sum	cell
PBE	↑	0	0	0	0	0	0	0	0
	↓	0.3526	0.4295	0.0025	0.0030	0.0038	0.1693	0.9607	1.0002
PBE+*U*	↑	0.0045	0.0028	0.0736	0.0124	0.0107	0.1567	0.2607	0.3337
	↓	0.2427	0.0198	0.0049	0.0029	0.0182	0.2594	0.5479	0.6643

[*)] The next to last column (sum) gives the sum of up and down spin contributions in previous columns, while the last column gives the result of the integration of total charge density between -0.4 eV and E_f, at the bottom of the conduction band. Let us note here quite different distribution of extra electron between the atoms, obtained by PBE and PBE+*U* approaches, although the net ferrimagnetic moment per unit cell is approximately the same for both exchange-correlation functionals used (on the order of $\sim 0.25\mu_B$, cf. previous table).

Figure captions

Fig. 1. (Color online) Polyhedral representation of the structure of olivine type $LiFePO_4$ (space group *Pnma*) viewed along the *b*-axis. Note that oxygen's site O(2) is colored in yellow.

Fig. 2. The image of the F-doped $LiFePO_4$/C obtained by FESEM.

Fig. 3. The size distribution of the particles in synthesized powder of the F-doped $LiFePO_4$/C.

Fig. 4. (Color online) The observed (•), calculated (-), and difference (bottom) X-ray diffraction data of the F-doped $LiFePO_4$/C taken at room temperature. Vertical markers bellow the diffraction patterns indicate positions of possible Bragg reflections.

Fig. 5. TEM image of the F-doped $LiFePO_4$/C powder.

Fig. 6. HRTEM image of the F-doped $LiFePO_4$/C powder. Amorphous carbon film, with a thickness of 3 nm, is deposited on the (121) crystal plane of the orthorhombic $LiFePO_4$.

Fig. 7. Charge-discharge curves of the F-doped $LiFePO_4$/C powder at different current rates and its rate performance (inset).

Fig. 8. (Color online) The antiferromagnetic total and partial DOS for $LiFePO_4$ calculated using the DFT with generalized gradient corrections (PBE), DFT with Coulomb correlations at Fe sites included (PBE+*U*, U_{eff}=4.3 eV), and TB-mBJ approach [31]. Zero energy is taken at the Fermi level. Red, green and blue curves designate the *s*, *p* and *d* states in respective atomic spheres, while gray curves stand for the interstitial region contributions.

Fig. 9. (Color online) The AF total and partial DOS for doped $LiFePO_{3.75}F_{0.25}$ calculated using the PBE and PBE+*U*, U_{eff}=4.3 eV. Red, green, blue, and gray curves designate the *s*, *p*, *d* and interstitial contributions.

Fig. 10. (Color online) Band structure of $LiFePO_4$ (left), $LiFePO_{3.75}F_{0.25}$ (middle), and DOS for doped compound (extreme right) in narrow region around the Fermi level (energy range E_f –2 eV to E_f + 2 eV)..

Fig. 11. (color online) The deformation of the FeO_6 octahedron caused by fluorine doping of $LiFePO_4$, *Up*: the distorted octahedron when O(2) oxygen is replaced by F (note that F doping affects the other Fe-O bond lengths), and *Down*: FeO_6 octahedron.

Fig. 12. (color online) The AF total DOS for $LiFePO_{3.75}F_{0.25}$ calculated using the GPAW: a real-space implementation of the projector augmented-wave method [33] with GGA corrections included [30]. DOS has been calculated with the Gaussian width of 0.2 eV or 0.05 eV (inset).

Fig. 13. (color online) The AF partial DOS calculated both for $LiFePO_4$ (iron and oxygen): (a) and (b), and for $LiFePO_{3.75}F_{0.25}$ (iron and fluorine): (c) and (d) by use of the GPAW with PBE corrections. Partial DOS has been calculated with the (Gaussian) width of 0.2 eV or 0.05 eV (insets). Oxygen's partial density of states changed insignificantly for the doped compound to deserve additional graphical presentation.

Fig. 14. (color online) Two isosurfaces of $\Delta\rho$ (see the text for the definition). Yellow contours stand for the electron density depletion (charge density difference for one negative value in arbitrary units), while the gray ones depict the electron density enhancement (positive density difference of the same absolute value in the same arbitrary units) within the unit cell. The volumes enclosed by gray and yellow contours, around the respective atoms, could be used as the

approximate measure of accumulation/depletion of the electron density (entirety of one extra electron) at these places in the unit cell.

Figure 1

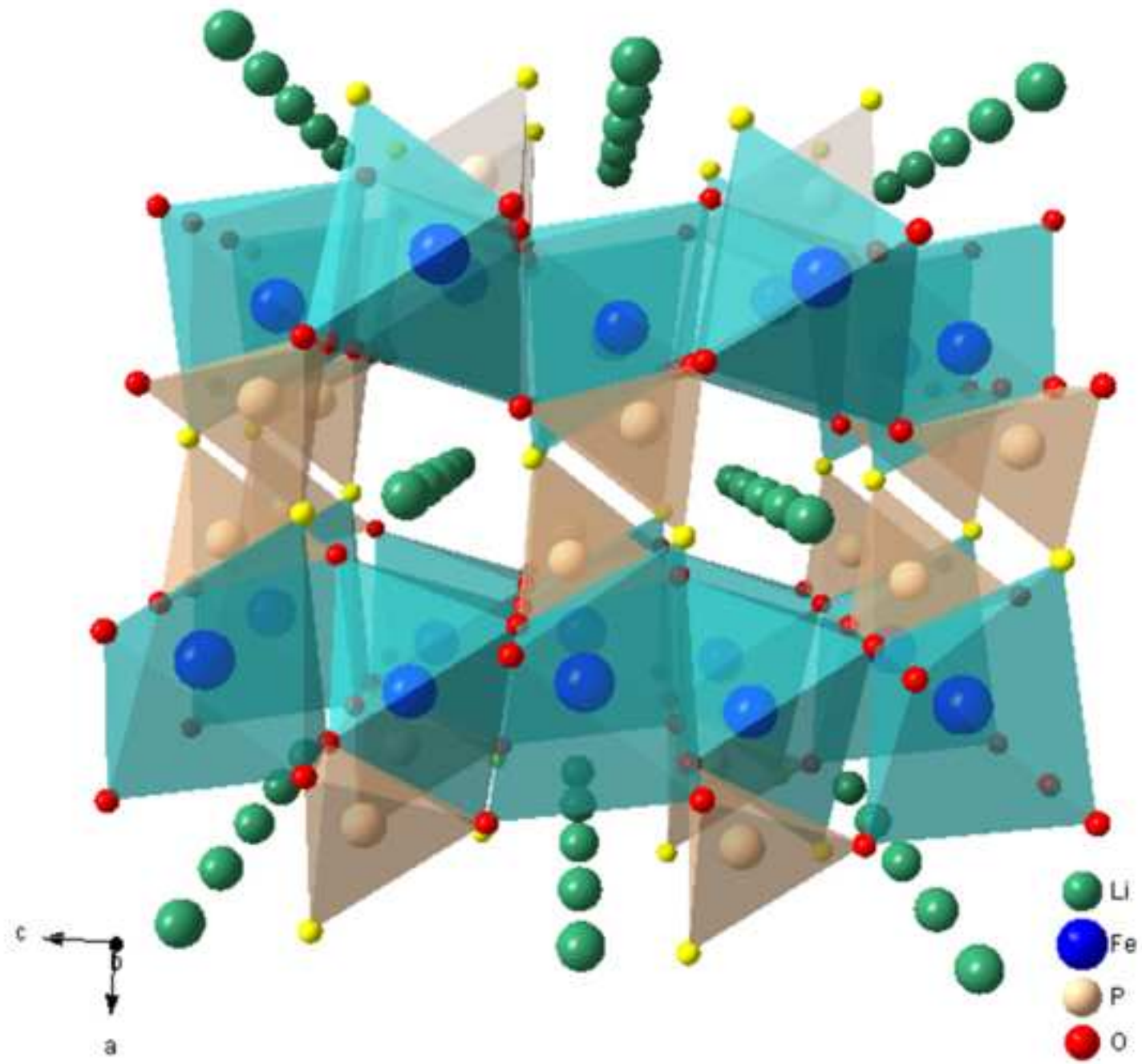

Figure 2

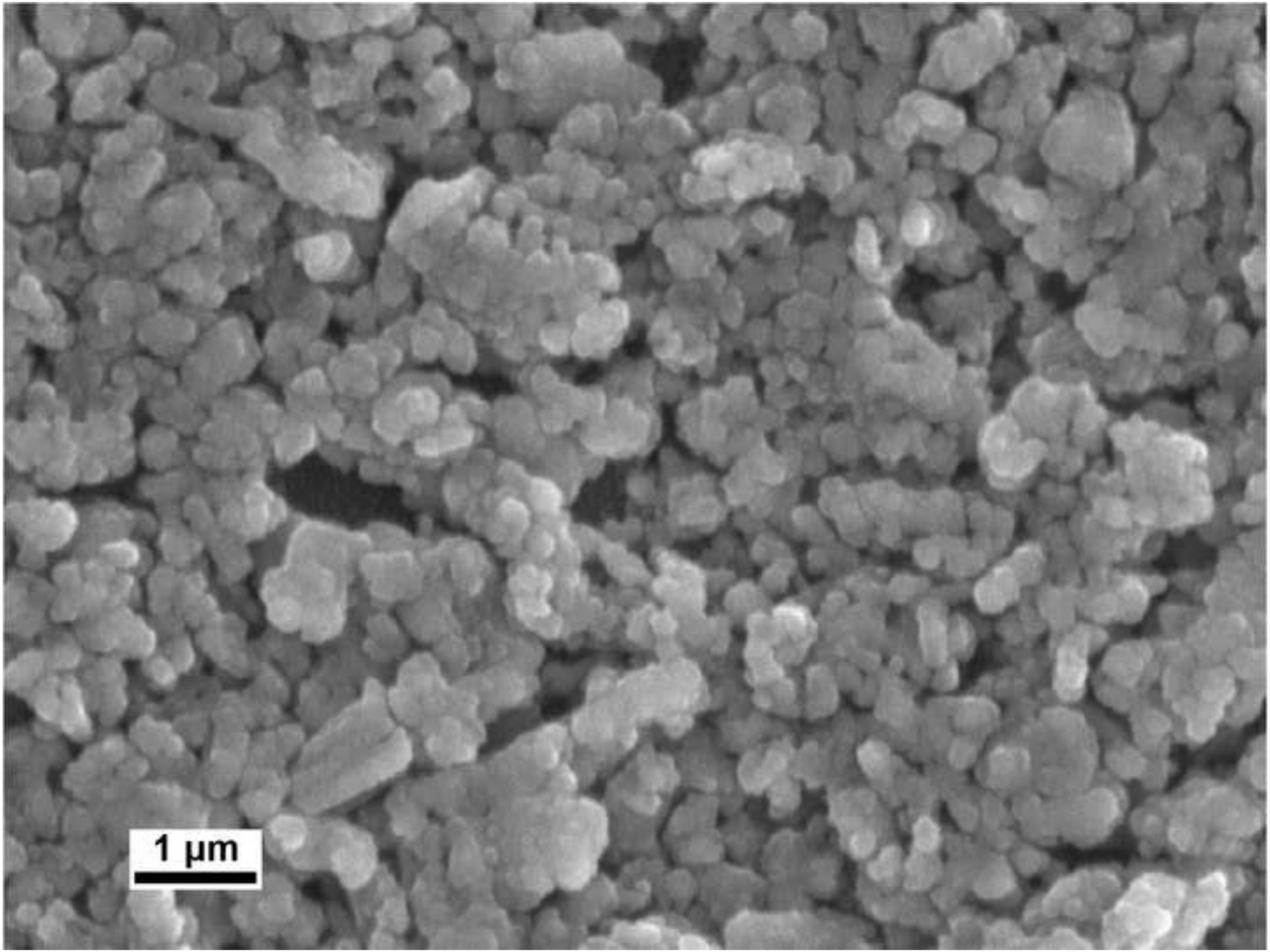

Figure 3

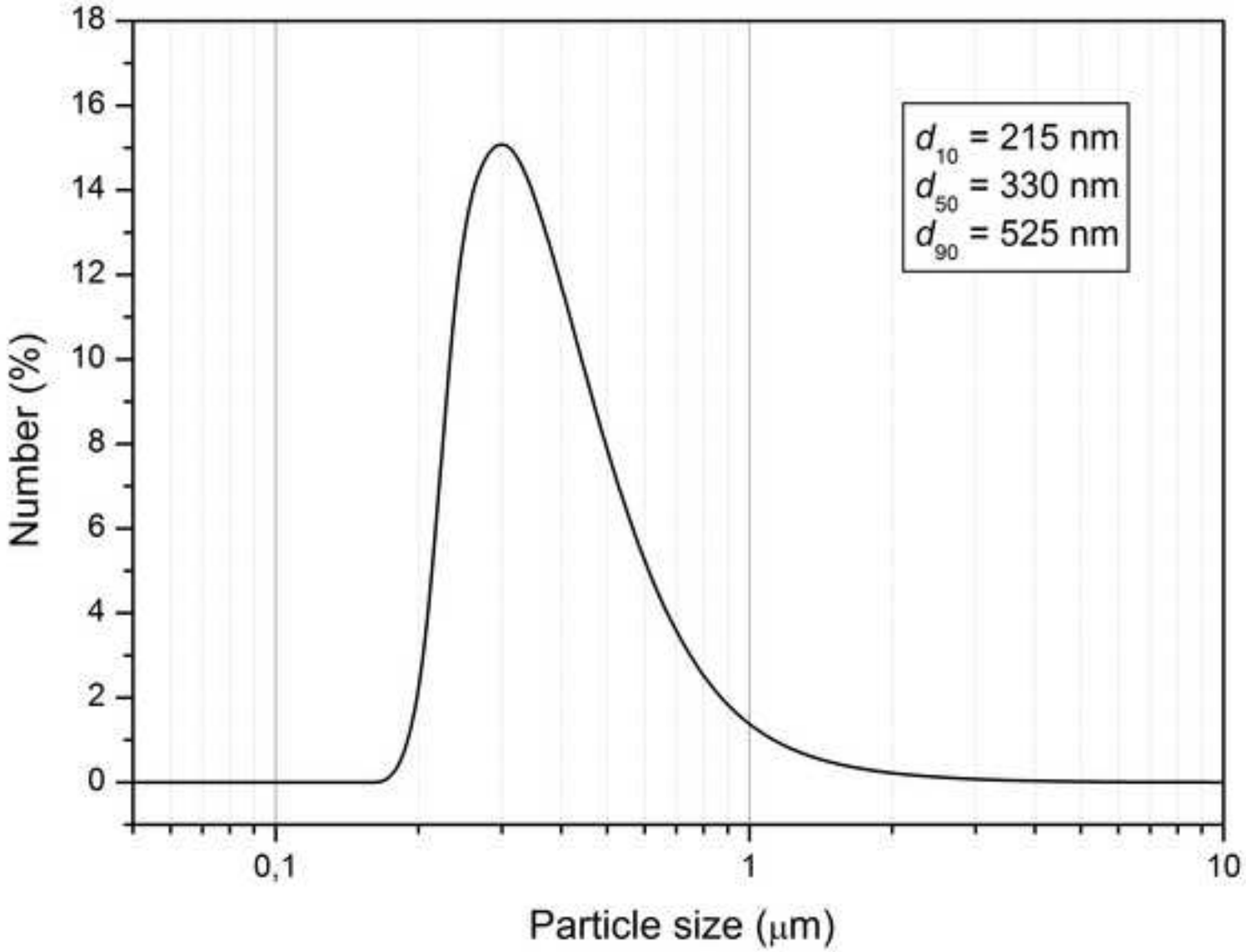
18
16
14
12
10
8
6
4
2
0
Number (%)
0,1
1
10
Particle size (μm)
d_{10} = 215 nm
d_{50} = 330 nm
d_{90} = 525 nm

Figure 4

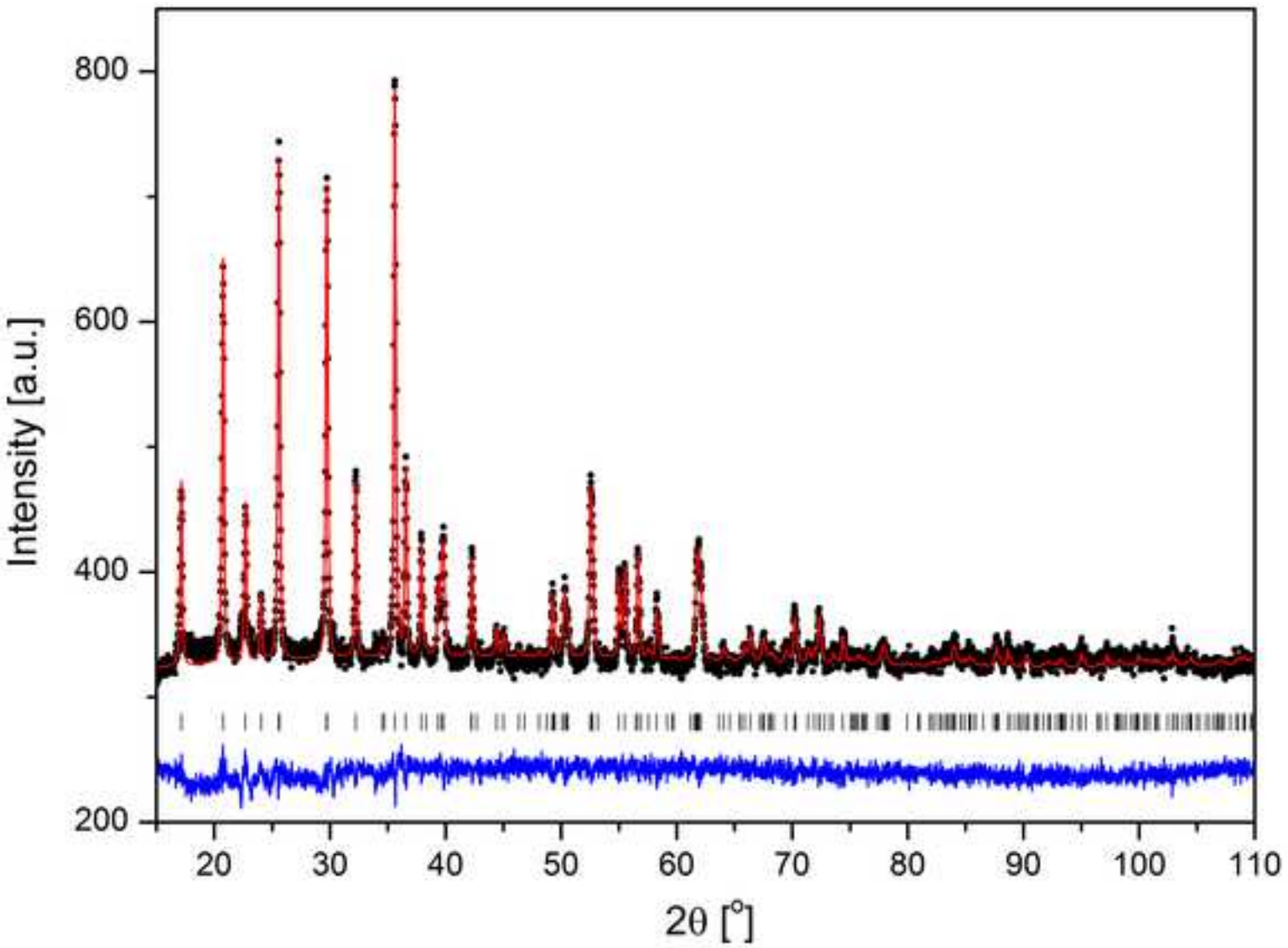

Figure 5

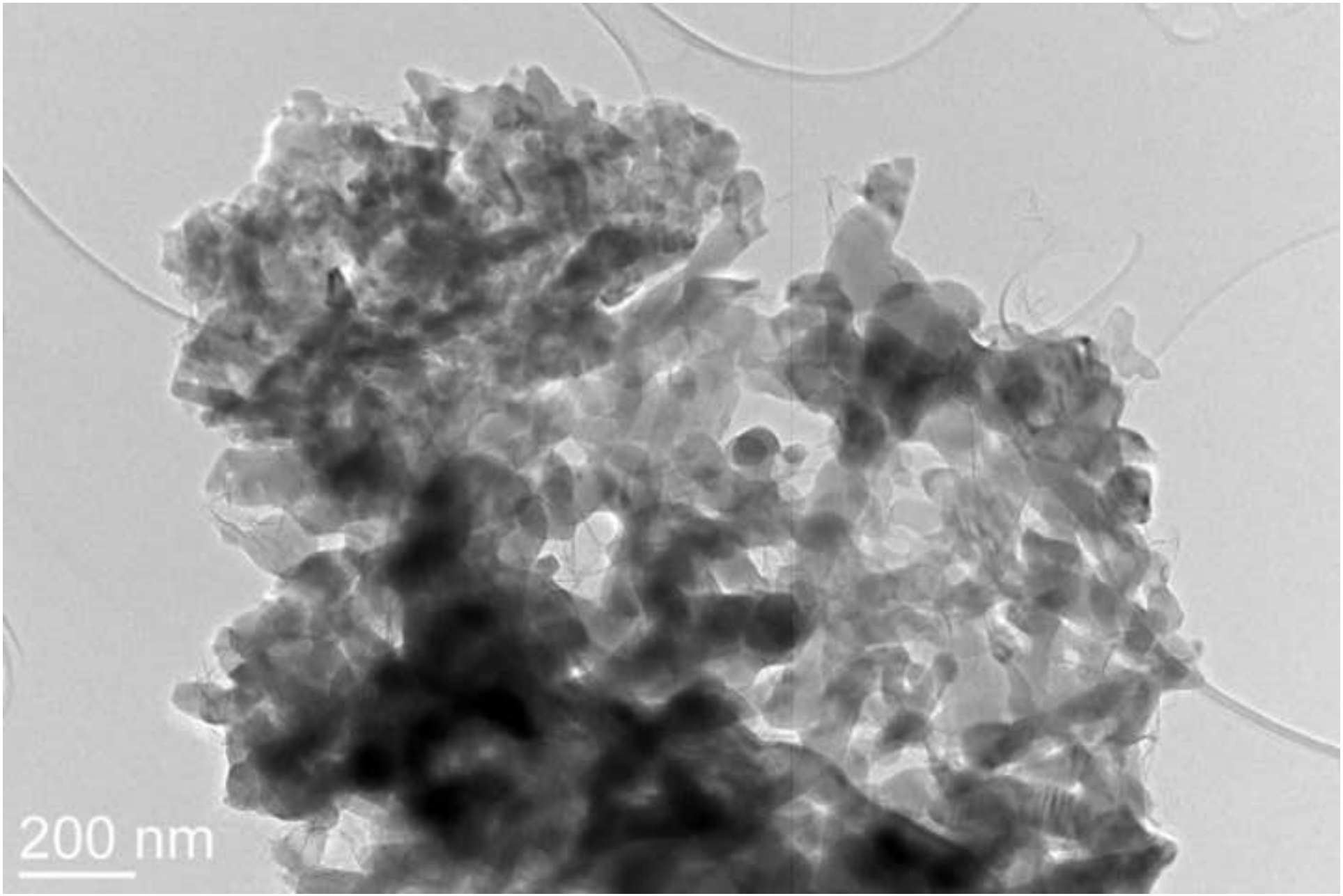

Figure 6

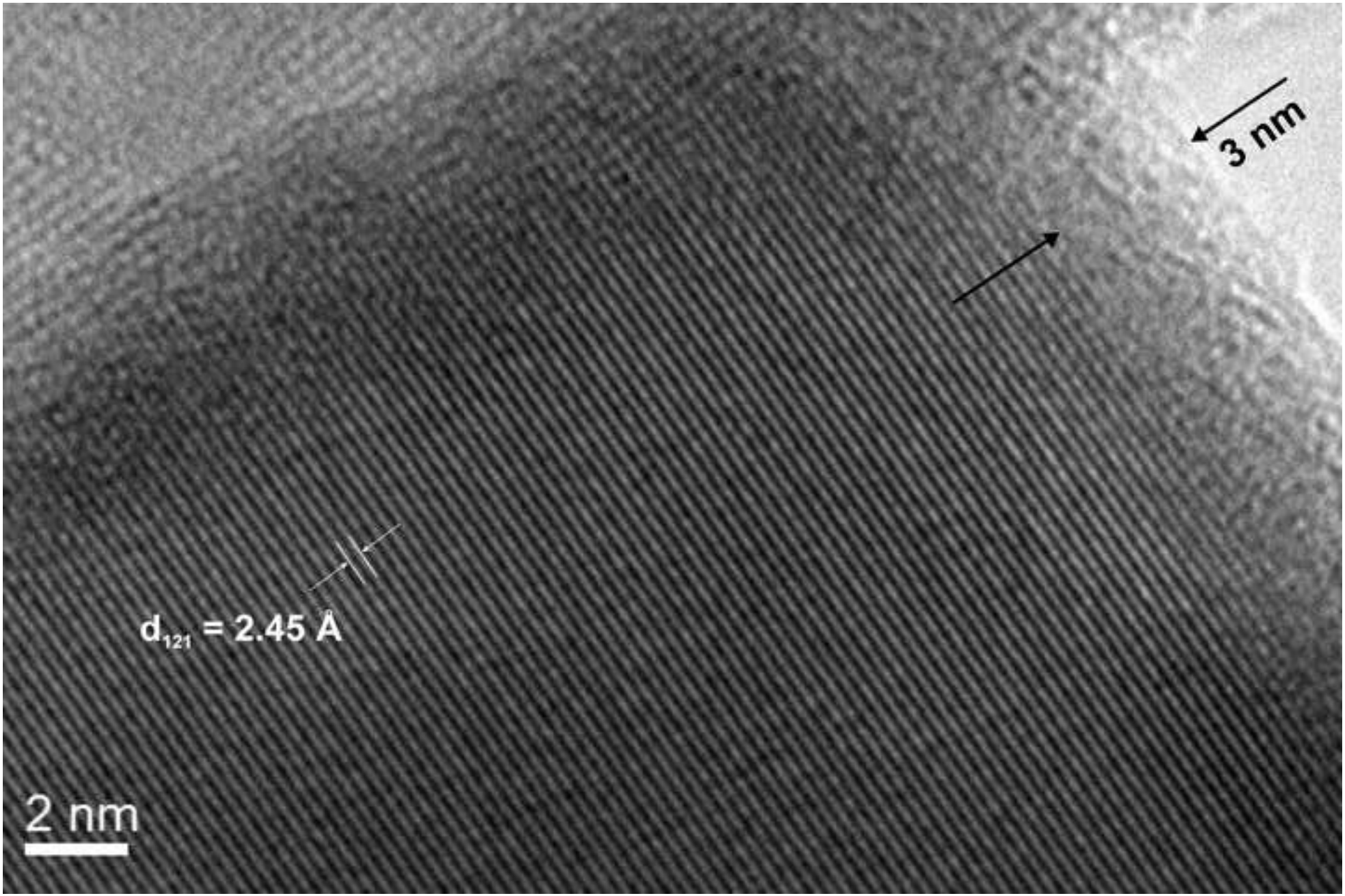

Figure 7

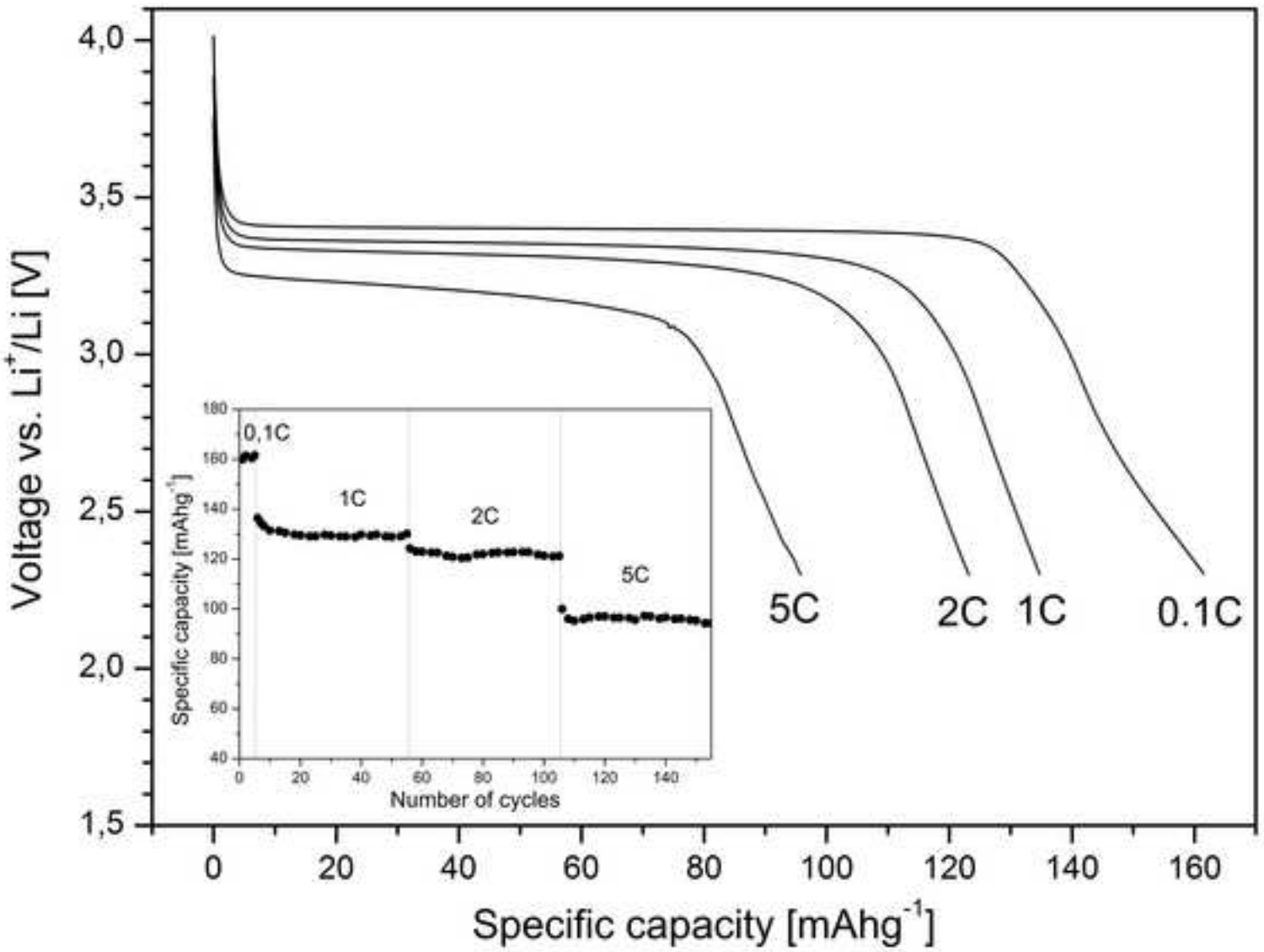
Voltage vs. Li+/Li [V]
4,0
3,5
3,0
2,5
2,0
1,5
0
20
40
60
80
100
120
140
160
Specific capacity [mAhg-1]
5C
2C
1C
0.1C
0,1C
1C
2C
5C
Specific capacity [mAhg-1]
Number of cycles

Figure 8

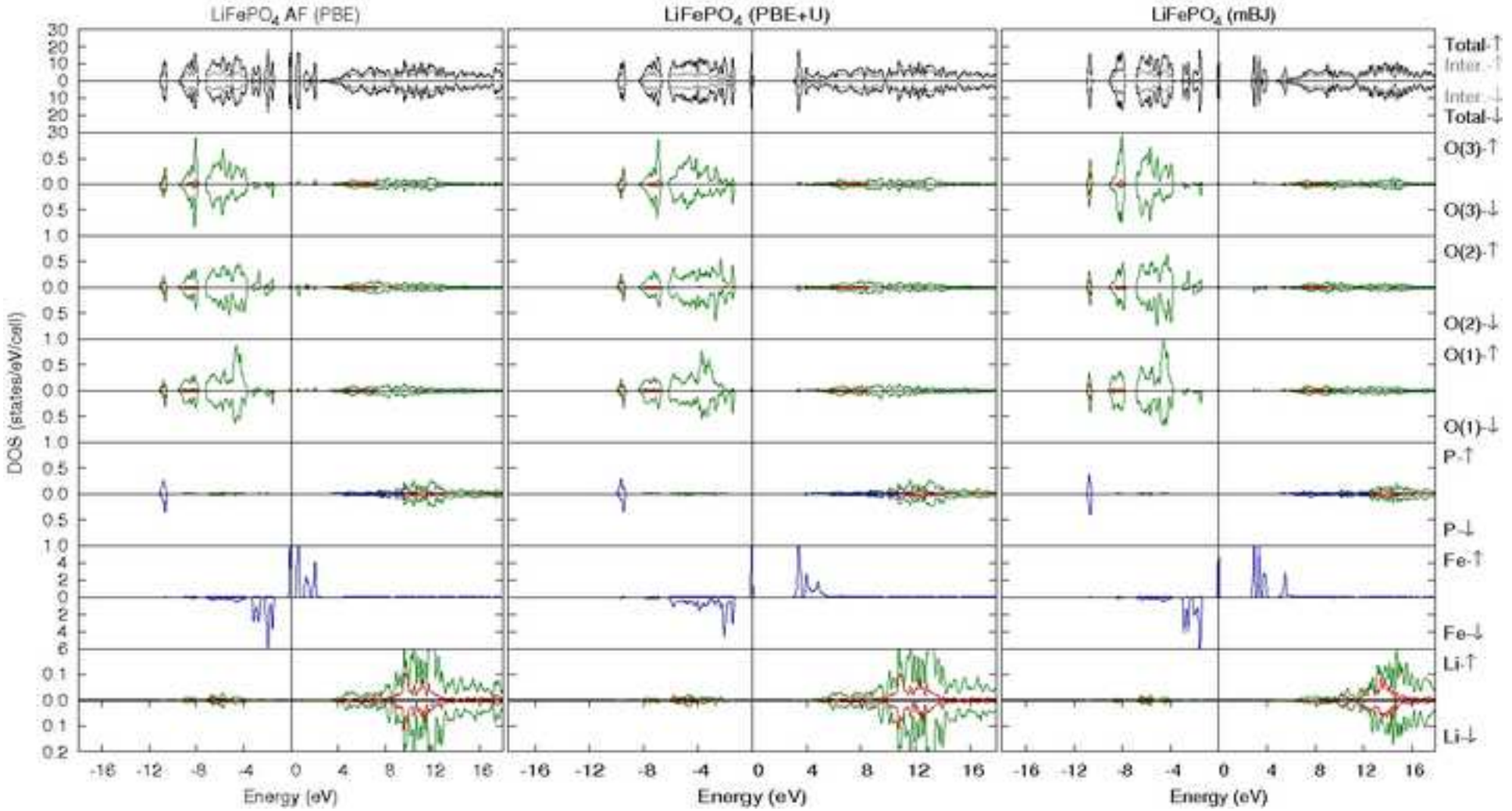
LiFePO4 AF (PBE)
LiFePO4 (PBE+U)
LiFePO4 (mBJ)
DOS (states/eV/cell)
Energy (eV)
Total-↑
Inter.-↑
Inter.-↓
Total-↓
O(3)-↑
O(3)-↓
O(2)-↑
O(2)-↓
O(1)-↑
O(1)-↓
P-↑
P-↓
Fe-↑
Fe-↓
Li-↑
Li-↓

Figure 9

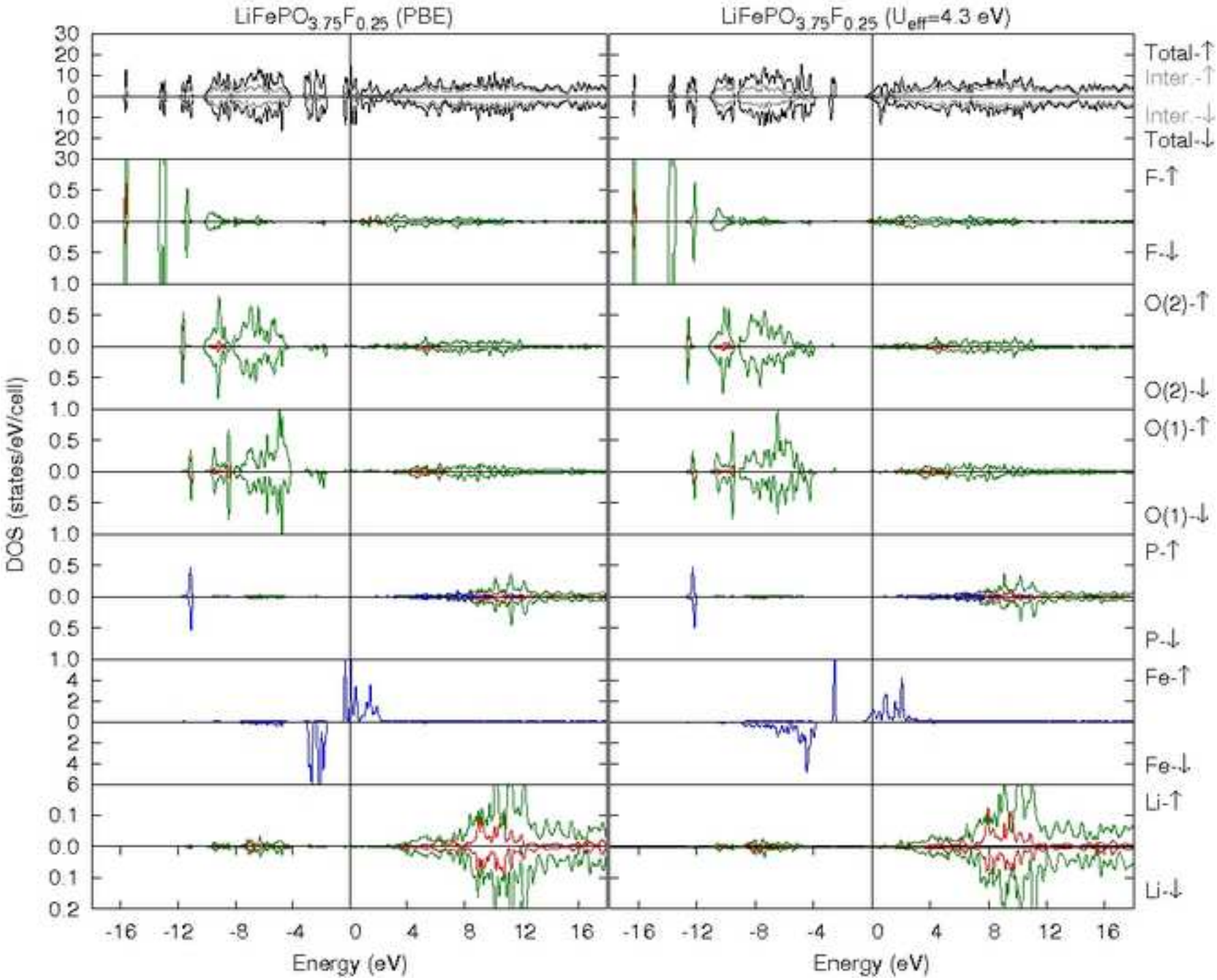
LiFePO3.75F0.25 (PBE)
LiFePO3.75F0.25 (Ueff=4.3 eV)
DOS (states/eV/cell)
Energy (eV)
Energy (eV)
Total-↑
Inter.-↑
Inter.-↓
Total-↓
F-↑
F-↓
O(2)-↑
O(2)-↓
O(1)-↑
O(1)-↓
P-↑
P-↓
Fe-↑
Fe-↓
Li-↑
Li-↓

Figure 10

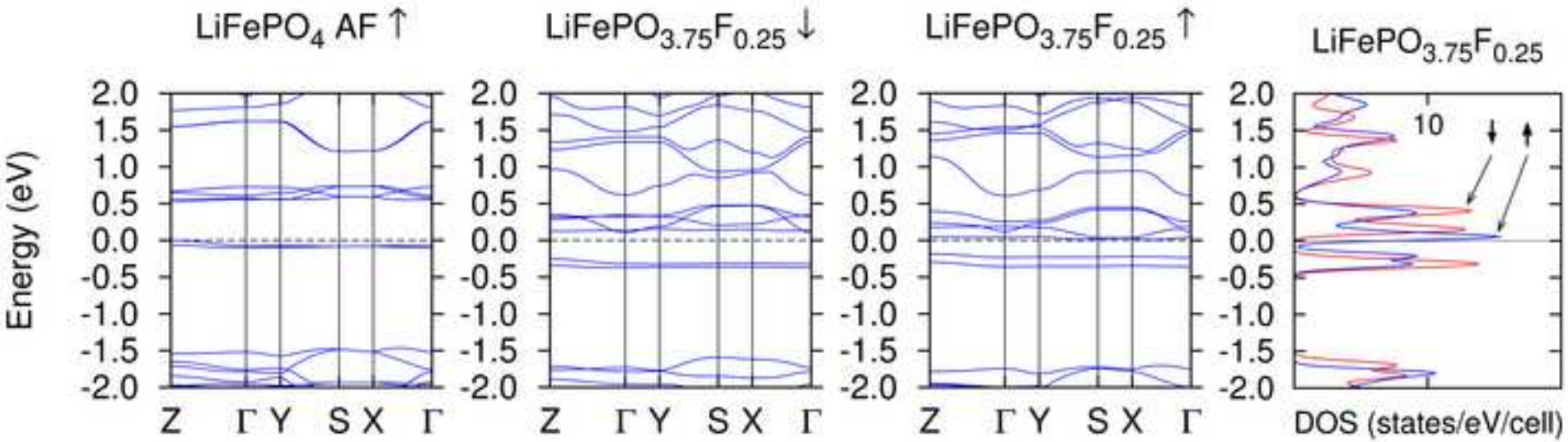
LiFePO4 AF ↑
LiFePO3.75F0.25 ↓
LiFePO3.75F0.25 ↑
LiFePO3.75F0.25
Energy (eV)
2.0
1.5
1.0
0.5
0.0
-0.5
-1.0
-1.5
-2.0
Z Γ Y S X Γ
10
DOS (states/eV/cell)

Figure 11

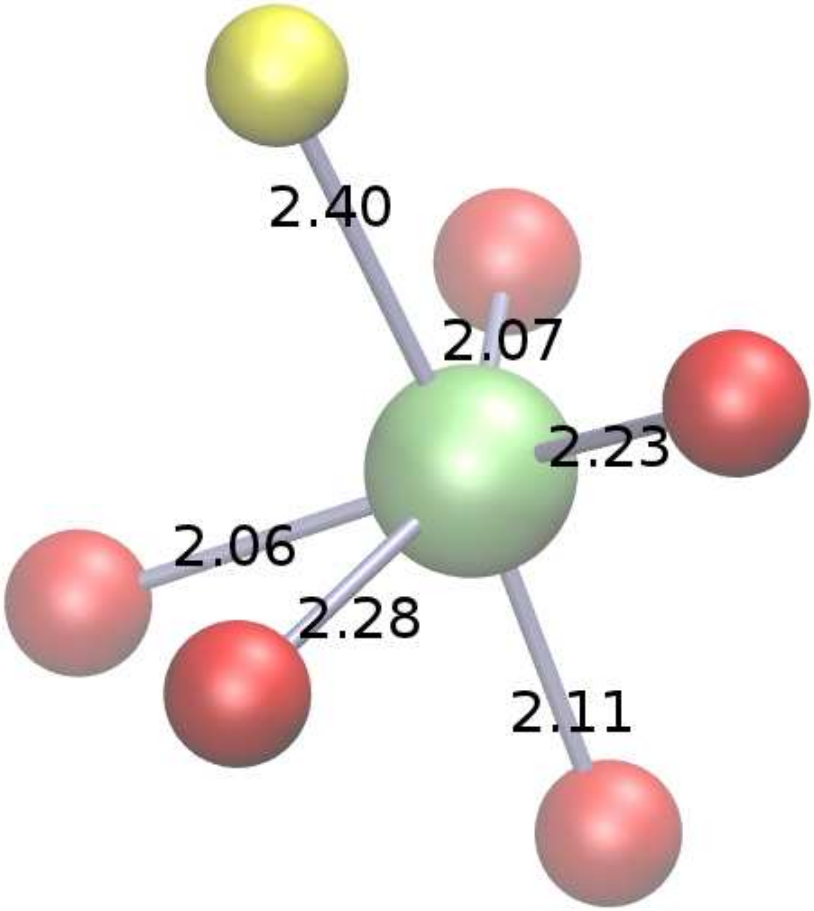

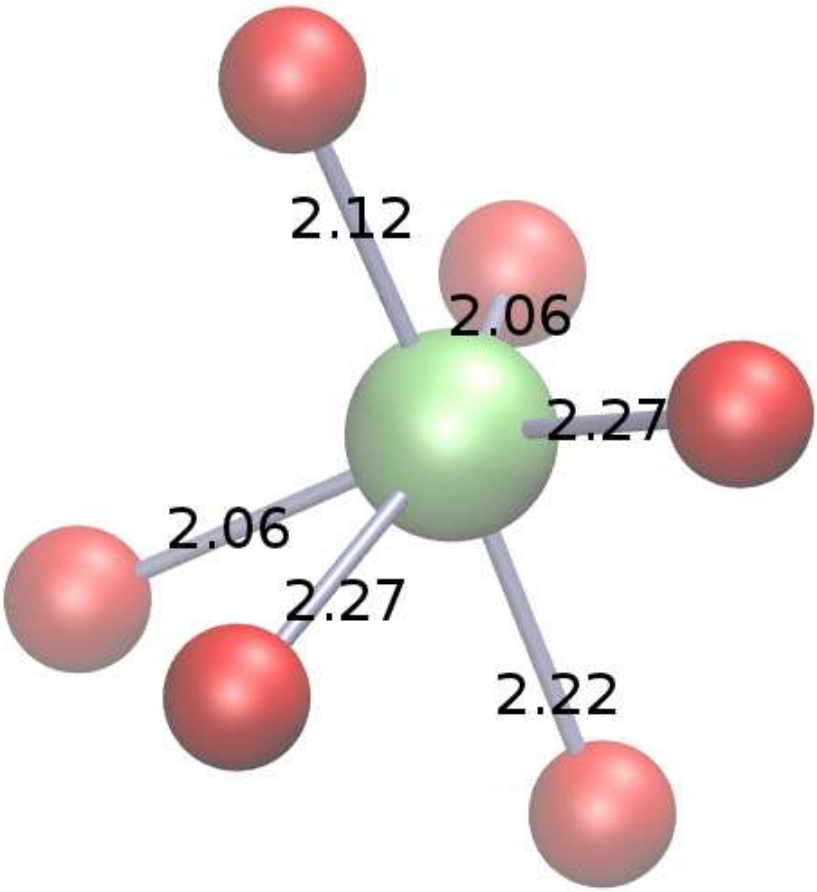

Figure 12

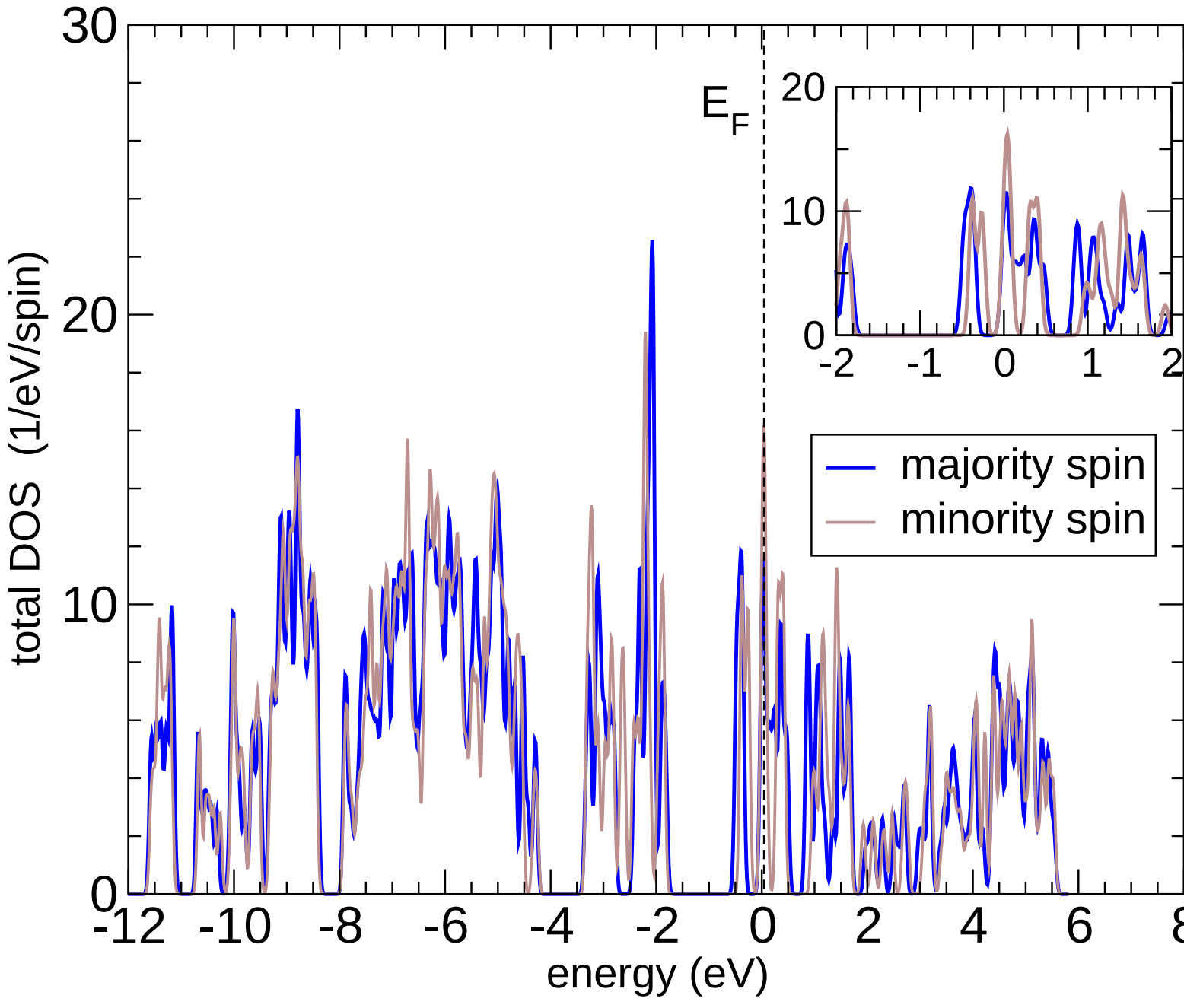
30
20
10
0
total DOS (1/eV/spin)
-12
-10
-8
-6
-4
-2
0
2
4
6
energy (eV)
E_F
20
10
0
-2
-1
0
1
2
majority spin
minority spin

Figure 13

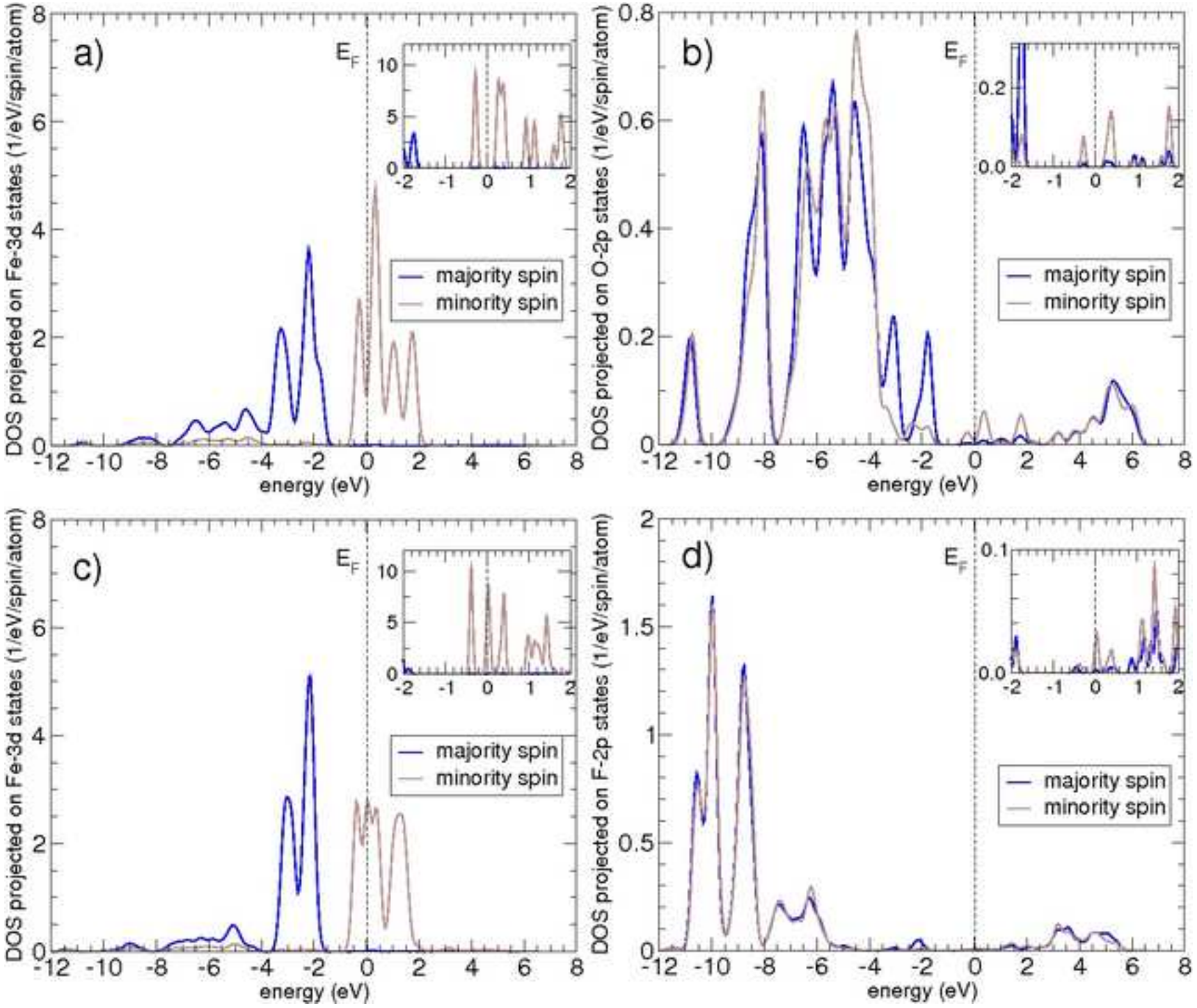
a)
b)
c)
d)
E_F
majority spin
minority spin
DOS projected on Fe-3d states (1/eV/spin/atom)
DOS projected on O-2p states (1/eV/spin/atom)
DOS projected on F-2p states (1/eV/spin/atom)
energy (eV)

Figure 14